LANGMUIR

pubs.acs.org/Langmuir Article

Impeded Molecular Reorganization by Polyethylene Glycol Conjugation Revealed by X-ray Reflectivity and Diffraction Measurements

Pin Zhang, Tiep Pham, Chang Liu, Paola Leon Plata, Joseph Kalkowski, Gang Cheng, Wei Bu, Binhua Lin, and Ying Liu*

Cite This: *Langmuir* 2020, 36, 7573−7581 Read Online

ACCESS | Metrics & More | Article Recommendations | Supporting Information

ABSTRACT: Polyethylene glycol (PEG) coatings have been widely applied in pharmaceutical and biomedical systems to prevent nonspecific protein absorption, increase vesicle blood circulation time, and sustain drug release. This study systematically investigated the planar interfacial organization of phospholipid monolayers containing various amounts of PEG conjugations before and after enzyme-catalyzed degradation of the lipids using X-ray reflectivity and grazing incidence X-ray diffraction techniques. Results showed that attaching PEG to the headgroup of the lipids up to 15 mol % had limited effects on molecular packing of the lipid monolayers in the condensed phase at the gas−liquid interface and negligible effects on the enzyme adsorption to the interface. After enzyme-catalyzed degradation, equimolar fatty acids and lyso PC were generated. The fatty acids together with the subphase Ca^{2+} self-assembled into highly organized multilayer domains at the interface. The X-ray measurements unambiguously revealed that the densely packed PEG markedly hindered microphase separation and formation of the palmitic acid−Ca^{2+} complexes.

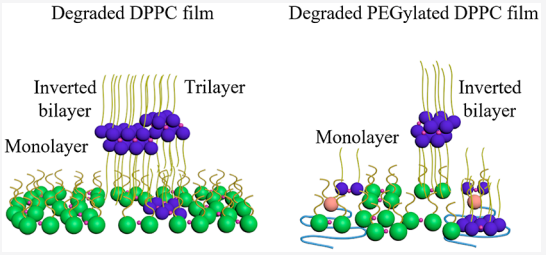

INTRODUCTION

Polyethylene glycol (PEG) is considered as a biocompatible polymer and has been approved by the U.S. Food and Drug Administration (FDA) for a wide range of applications in biomedicine and medical devices[1,2] due to its low toxicity,[3,4] lack of immunogenicity,[5] and excellent solubility in aqueous solution.[6] PEGylation (conjugating directly with drug molecules or entrapping PEG on the surface of drug-carriers) has been reported to increase hydrophobic drug stability and solubility and therefore improve drug pharmacokinetics and biodistribution through "stealth effects". PEGylation protects drugs or drug carriers from nonspecific protein adsorption and thus from being recognized and rapidly cleared by the mononuclear phagocyte system (MPS). This prolongs their blood circulation and increases the probability of the active compounds reaching the target sites.[7,8]

The mechanisms of the stealth effects have been largely attributed to the repulsion provided by the hydrophilic polymer brushes that sterically preclude interaction of drug carriers with surrounding blood proteins[9−11] and other drug carriers.[12−14] Several studies have suggested a more complicated mechanism, in which the stealth effects required the adsorption of specific proteins (such as clusterins), forming a protein corona to prevent nonspecific cellular uptake.[15,16] However, studies using phospholipids and secretory phospholipase A2 ($sPLA_2$) as a model system indicated contradictory results of enhanced degradation of PEGylated liposomes compared to liposomes without PEG, which also showed a positive correlation between liposome degradation enhancement and the PEG molecular weight and density.[17−19] Zhu et al.[20] attributed this enhancement to the negative charges induced by PEGylation, while Majewski et al.[21,22] and Halperin et al.[23] suggested that protrusion of the neighboring lipids around the PEGylated lipids was the predominant reason. For a liposome system, the effects of PEGylation likely combine complicated factors of molecular interaction, membrane kinetics, and geometric packing. For example, PEGylation can induce osmotic imbalance[24] and membrane fusion in liposomes due to their high curvature. In addition, inclusion of more PEG-grafted phospholipids tended to reduce liposome size and changed the morphologies of lipid aggregates,[18,25−27] which may have enhanced enzyme activity in catalyzing the degradation of the PEGylated liposomes.[28] In order to decouple the effects of curvature, this study focuses on revealing the effects of PEG on lipid packing, enzyme adsorption, and lipid degradation in lipid monolayers at the

Received: April 23, 2020
Revised: June 2, 2020
Published: June 5, 2020

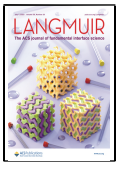

https://dx.doi.org/10.1021/acs.langmuir.0c01202
Langmuir 2020, 36, 7573−7581

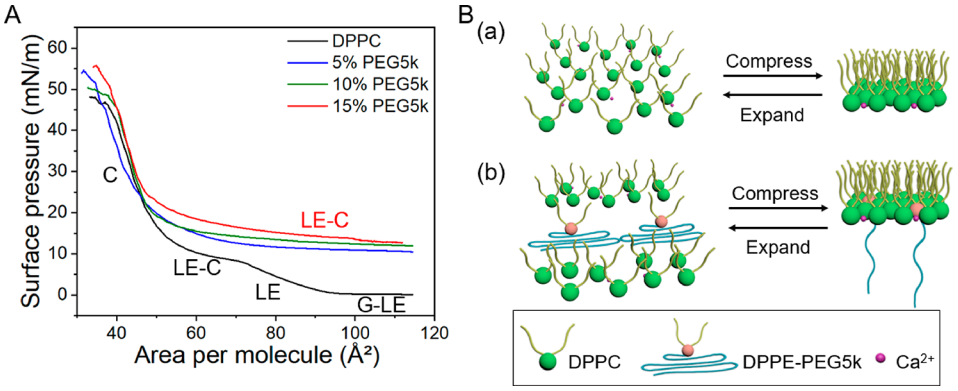

Figure 1. Representative surface pressure-mean molecular area isotherms of DPPC and DPPC with 5%, 10%, and 15% DPPE-PEG5k on a Ca buffer. During continuous compression, the DPPC monolayer exhibited a four-phase transition. With DPPE-PEG5k, the starting pressure was high, and the curves began with the LE-C phase. (B) Schematics representing the molecular organization of (a) DPPC and (b) binary mixture of DPPC and DPPE-PEG5k monolayers.

planar gas−liquid interface. A model enzyme, $sPLA_2$ was used for the study, because its intrinsic overexpression in various diseases has potential to be employed as a therapeutic strategy for diagnosis and treatment.[29−31] Molecular-level quantification of the monolayer packing structure and degradation was achieved by employing X-ray reflectivity (XR) and grazing incidence X-ray diffraction (GIXD) techniques. The results provide a fundamental understanding of the effects of the hydrophilic polymer brushes on lipid and enzyme interaction that will support mechanism-orientated design of lipid-based drug delivery systems for particular therapeutic purposes.

MATERIALS AND METHODS

Materials and Reagents. Lipids, including 1,2-dipalmitoyl-*sn*-glycero-3-phosphocholine (DPPC), 1-palmitoyl-2-hydroxy-*sn*-glycero-3-phosphocholine (lysoPC), and 1,2-dipalmitoyl-*sn*-glycero-3-phosphoethanolamine-*N*-[methoxy (polyethylene glycol) 5000]-ammonium salt (DPPE-PEG5k) were purchased from Avanti Polar Lipids. Palmitic acid (PA), calcium chloride dihydrate, and $sPLA_2$ extracted from honeybee (*Apis mellifera*) venom were purchased from Sigma-Aldrich. Two buffer solutions were used as the subphases in the Langmuir trough. The Ca-free buffer contained 8 mM tris (purchased from Fisher) and the Ca buffer contained 8 mM tris and 5 mM $CaCl_2$. For both buffer solutions, pH values were adjusted to 7.4 by adding diluted hydrochloric acid with a concentration of 3.7 v%. Organic solvents, including methanol, ethanol, and chloroform, were purchased from Sigma-Aldrich. Deionized water to 18.2 MΩ (MILLIPORE) was used in all experiments. All chemicals were purchased at standard grades and used as-received.

Surface Pressure-Mean Molecular Area Isotherms of Phospholipid Monolayers. Surface pressure-mean molecular area isotherms of the monolayers on the Ca buffer were measured using a Langmuir trough (51 × 155 mm^2, KSV NIMA, Biolin Scientific). The temperature of the subphase was monitored by a thermocouple inserted in the subphase and controlled by a water circulation system (Anova Scientific) at 23 ± 0.5 °C. Interfacial tension was measured by a platinum Wilhelmy plate hooked to a wire that was attached to a film balance. Lipid samples were dissolved in chloroform and stored at −20 °C. Before each measurement, the trough was cleaned thoroughly, which was confirmed by a surface pressure fluctuation less than ±0.2 mN/m throughout the entire surface area change. A lipid sample was then spread dropwise on the subphase using a syringe. After allowing 10 min for the solvent to evaporate, the phospholipid monolayer was compressed by two symmetric barriers, each moving at 1 mm/min until the collapse point of the monolayer was reached. The surface pressure-mean molecular area isotherm for the lipid monolayer was recorded during compression.

X-ray Measurements. XR and GIXD experiments were conducted using a Langmuir trough integrated with the synchrotron X-ray beamline at the National Science Foundation's (NSF's) ChemMatCARS (sector 15C of Advanced Photon Sources) at Argonne National Laboratory. Details of the experimental setup were described in our previous studies.[32−34] The X-ray wavelength was 1.24 Å, and all experiments were conducted at about 22.7 °C.

Before each experiment, the trough was cleaned, and the lipid sample was spread at the gas−liquid interface by the same method as described in the previous section. Immediately after spreading the lipids, the box containing the trough was sealed and purged with helium gas until the concentration of oxygen inside the box was less than 2%. The monolayer was then compressed by a one-sided barrier at a rate of 6.4 mm/min until the surface pressure reached 25 mN/m. The XR and GIXD measurements of the lipid monolayer were conducted at a constant pressure of 25 mN/m, which was maintained by autoadjustment of the position of the barrier. After these measurements, the barrier position was fixed to maintain a constant area, and $sPLA_2$ solution was injected into the subphase to reach a final concentration of 10 ng/mL. The subphase was then gently stirred for 1 h, and then another hour was allowed for the surface to settle. The XR and GIXD measurements were conducted to quantify enzyme adsorption and enzyme-catalyzed lipid degradation at the film positions previously unexposed to X-ray.

X-RAY DATA ANALYSIS

XR measurement probes the interfacial organization of films in the direction normal to the interface. By varying the incident angles, the reflected X-ray was recorded. The X-ray reflectivity (R) was normalized by the Fresnel reflectivity (R_F), whose electron density profile represents an ideal, smooth, and flat air−water interface.[35] Using the Parratt formalism,[36] the normalized X-ray reflectivity (R/R_F) was fitted by using a box-model with an electron density presented by a sum of error functions:

$$\rho(z) = \frac{1}{2}\sum_{i=0}^{N} \mathrm{erf}\left(\frac{z - z_i}{\sqrt{2}\,\sigma_i}\right) \times (\rho_i - \rho_{i+1}) + \frac{\rho_0}{2} \quad (1)$$

where erf represents an error function; N is the number of slabs across the interface; z_i and σ_i are the position and roughness of the i^{th} interface, respectively; ρ_i is the electron density of the i^{th} slab; and ρ_0 is the electron density of the subphase.

For DPPC monolayer, a two-box model (one box representing the headgroup regions and one representing the tails) with the same roughness of σ for all interfaces was

https://dx.doi.org/10.1021/acs.langmuir.0c01202
Langmuir 2020, 36, 7573−7581

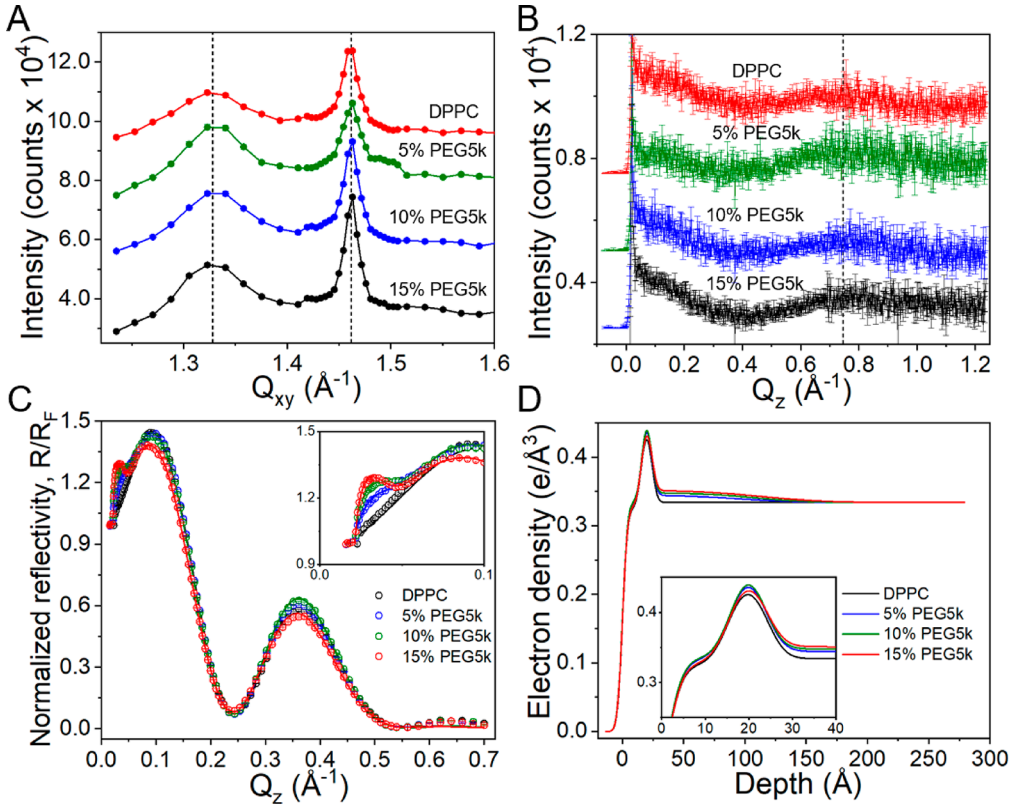

Figure 2. Effects of PEGylation on interfacial organization of DPPC monolayers on Ca buffer at a constant surface pressure of 25 mN/m. (A) Bragg peaks and (B) Bragg rods obtained from monolayers of DPPC and DPPC with 5%, 10%, and 15% of DPPE-PEG5k. In both plots, data are offset for clarity. The dashed lines in A and B indicate the peak positions of the Bragg peaks and the out-plane Bragg rods of the DPPC monolayer. (C) Normalized X-ray reflectivity. The insert in C amplifies the low Q_z region (0 to 0.1 Å^{-1}) to show the peak induced by PEG moieties. Solid lines are best fits obtained using box models. (D) Electron density profiles. The insert in D amplifies the electron density profiles about the lipid headgroup regions.

applied to fit the XR data. For the monolayers containing PEGylated lipids, a three-box model with an additional box representing the PEG layer below the headgroup region was used to achieve a better fit to the XR data. Furthermore, considering the combined effects of capillary waves and the decay of the PEG layer into the aqueous phase, a flexible roughness (σ_{PEG}) was included between the PEG−liquid interface while the roughness of the other interfaces was fixed.

After lipid film degradation catalyzed by sPLA$_2$, domains of degraded products emerged.[32] Thus, a multiphase box model with incoherent addition of reflectivity from different domains was used to fit the reflectivity data,[37]

$$R_{\text{incoherent}} = \Sigma C_j R_j \quad (2)$$

where C_j is the fractional interfacial coverage of the j^{th} domain, $\Sigma\ C_j = 1$, and R_j is the reflectivity from the j^{th} domain.

Two-dimensional GIXD data were obtained using an area detector (Pilatus 100 K) to record the scattered X-ray intensity with the variation of both horizontal wave vector Q_{xy} (parallel to the interface) and vertical wave vector Q_z (normal to the interface). Integrating the two-dimensional GIXD intensities over the Q_z range and Q_{xy} range then resulted in Bragg peaks and Bragg rods, respectively. The Bragg peaks were fitted using Gaussian functions, while the Bragg rods of the out-plane peaks were fitted using distorted wave Born approximation (DWBA).[38−40]

RESULTS AND DISCUSSION

Effects of PEGylation on the Interfacial Organization of Phospholipid Monolayers. Representative surface pressure-mean molecular area isotherms of DPPC films with various molar fractions of DPPE-PEG5k on the Ca buffer are shown in Figure 1. In general, under continuous compression, the mean molecular area of the monolayers decreased, and the surface pressure increased before the collapse points were reached.[41] For the DPPC monolayer, the slope of the increasing surface pressure displayed four distinct regions that correspond to four phases: gas and liquid-expanded transition phase (G-LE), liquid-expanded (LE) phase, liquid-expanded and condensed (LE-C) transition phase, and condensed (C) phase. When DPPE-PEG5k was included in the film, the surface pressure before compression was about 10 mN/m, and the film was in the LE-C phase. This high surface pressure may have been due to the large volume of PEG moieties pushing the surrounding lipid molecules into tight packing. When more DPPE-PEG5k lipids were present, the starting surface pressure and the surface pressure of the LE-C transition phase became slightly higher. Notably, the isotherms of all monolayers merged in the C phase, indicating that PEGylation had limited effects on molecular packing of lipid films in the C phase, which is consistent with the results of other isotherm studies of binary mixtures of lipids with shorter PEGylated lipids such as DPPC with DPPE-PEG2k[42] and 1,2-distearoyl-*sn*-glycero-3-phosphoethanolamine (DSPE) with

https://dx.doi.org/10.1021/acs.langmuir.0c01202
Langmuir 2020, 36, 7573−7581

Table 1. Structural Parameters Resulted from the Model Fitting of XR Data for Monolayers of DPPC and DPPC with 5%, 10%, and 15% DPPE-PEG5k at the Gas−Liquid Interface[a]

parameters	DPPC	5% PEG5k	10% PEG5k	15% PEG5k
σ (Å)	$3.3^{+0.2}_{-0.1}$	$3.4^{+0.1}_{-0.1}$	$3.4^{+0.2}_{-0.1}$	$3.4^{+0.1}_{-0.1}$
d_{tail} (Å)	$15.2^{+0.4}_{-0.2}$	$15.8^{+2.1}_{-0.4}$	$16.1^{+1.8}_{-0.5}$	$15.5^{+0.4}_{-0.2}$
ρ_{tail} (e/Å^3)	$0.325^{+0.003}_{-0.004}$	$0.332^{+0.008}_{-0.003}$	$0.334^{+0.006}_{-0.003}$	$0.328^{+0.003}_{-0.003}$
d_{head} (Å)	$8.9^{+0.2}_{-1.1}$	$7.8^{+0.1}_{-3.6}$	$7.4^{+0.3}_{-3.8}$	$8.5^{+0.2}_{-0.9}$
ρ_{head} (e/Å^3)	$0.446^{+0.039}_{-0.004}$	$0.468^{+0.018}_{-0.008}$	$0.478^{+0.112}_{-0.012}$	$0.454^{+0.007}_{-0.007}$
d_{PEG} (Å)		$70.8^{+8.5}_{-13.0}$	$84.1^{+5.5}_{-5.1}$	$89.3^{+7.5}_{-5.5}$
ρ_{PEG} (e/Å^3)		$0.345^{+0.002}_{-0.003}$	$0.348^{+0.002}_{-0.002}$	$0.35^{+0.002}_{1-0.003}$
σ_{PEG} (Å)		$39.2^{+10.8}_{-10.5}$	$34.4^{+6.5}_{-5.6}$	$41.5^{+7.5}_{-6.3}$
χ^2	37	9.1	10.4	13.7

[a]The electron density of the aqueous subphase was 0.334 e/Å^3 for the Ca buffer. The error bar for each parameter was calculated based on one standard deviation from the best fit value. The PEG layer thickness was constrained to the range of 20−100 Å, and the roughness (σ) between the PEG layer and the aqueous subphase was constrained to 0−50 Å. The electron density of alkyl chain tail was constrained to the range of 0−0.34 e/Å^3.

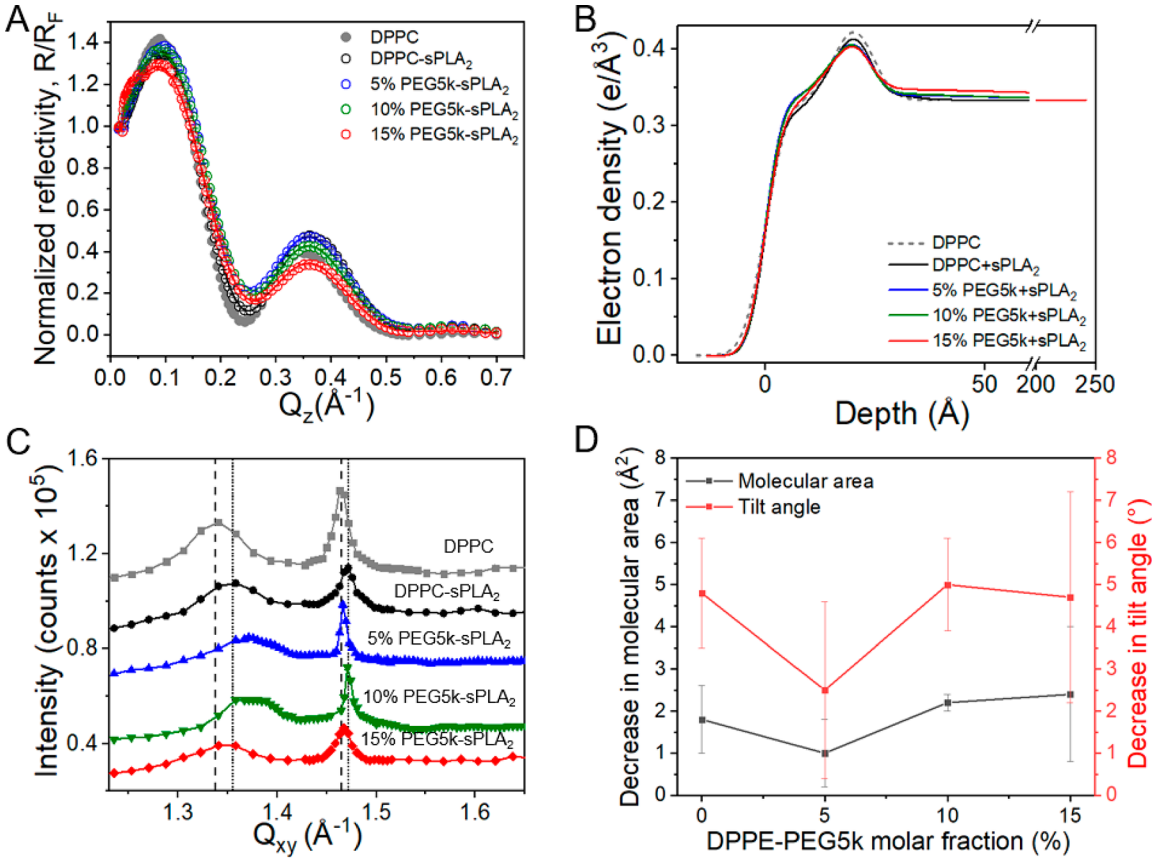

Figure 3. Effects of PEGylation on sPLA$_2$ adsorption to lipid monolayers on Ca-free buffer at constant surface area. (A) Normalized reflectivity of the monolayers of DPPC and DPPC with 5%, 10%, and 15% DPPE-PEG5k after sPLA$_2$ adsorption. (B) Electron density profiles resulting from fitting the curves of Figure 3A. Structural parameters are listed in Table S2. (C) Representative Bragg peaks of lipid films after sPLA$_2$ adsorption. The curves are offset for clarity. (D) The decrease in mean molecular area of lipids and tilt angle of tails after sPLA$_2$ adsorption. The results were averaged from two independent measurements, and the structural parameters obtained from GIXD are listed in Table S3.

1,2-distearoyl-*sn*-glycero-3-phosphoethanolamine-*N*-[methoxy (polyethylene glycol) 2000] (DSPE-PEG2k).[21]

Molecular packing structures of the monolayers of DPPC and DPPC with 5%, 10%, and 15% DPPE-PEG5k at a constant surface pressure of 25 mN/m at the gas−liquid interface were quantified using GIXD and XR. The measurements obtained from the same monolayer at different regions were highly repeatable and consistent, indicating relatively uniform monolayers. The GIXD results of all four monolayers exhibited similar Bragg peak and rod positions and widths: an out-plane Bragg peak at $Q_{xy} \approx 1.33$ Å^{-1}, an in-plane Bragg peak at a higher $Q_{xy} \approx 1.48$ Å^{-1} (Figure 2A), and a Bragg rod for the out-plane peak at $Q_z \approx 0.74$ Å^{-1} (Figure 2B). The Bragg peak and Bragg rod patterns indicated that the phospholipid tails in all four films had a nearest neighbor (NN) packing structure with a mean molecular area of about 48.6 Å^2 and a tilt angle of about 34°. Related structural parameters for each film are listed in Table S1 of the Supporting Information (SI). The GIXD results suggest that PEGylation had negligible effects on the

https://dx.doi.org/10.1021/acs.langmuir.0c01202
Langmuir 2020, 36, 7573−7581

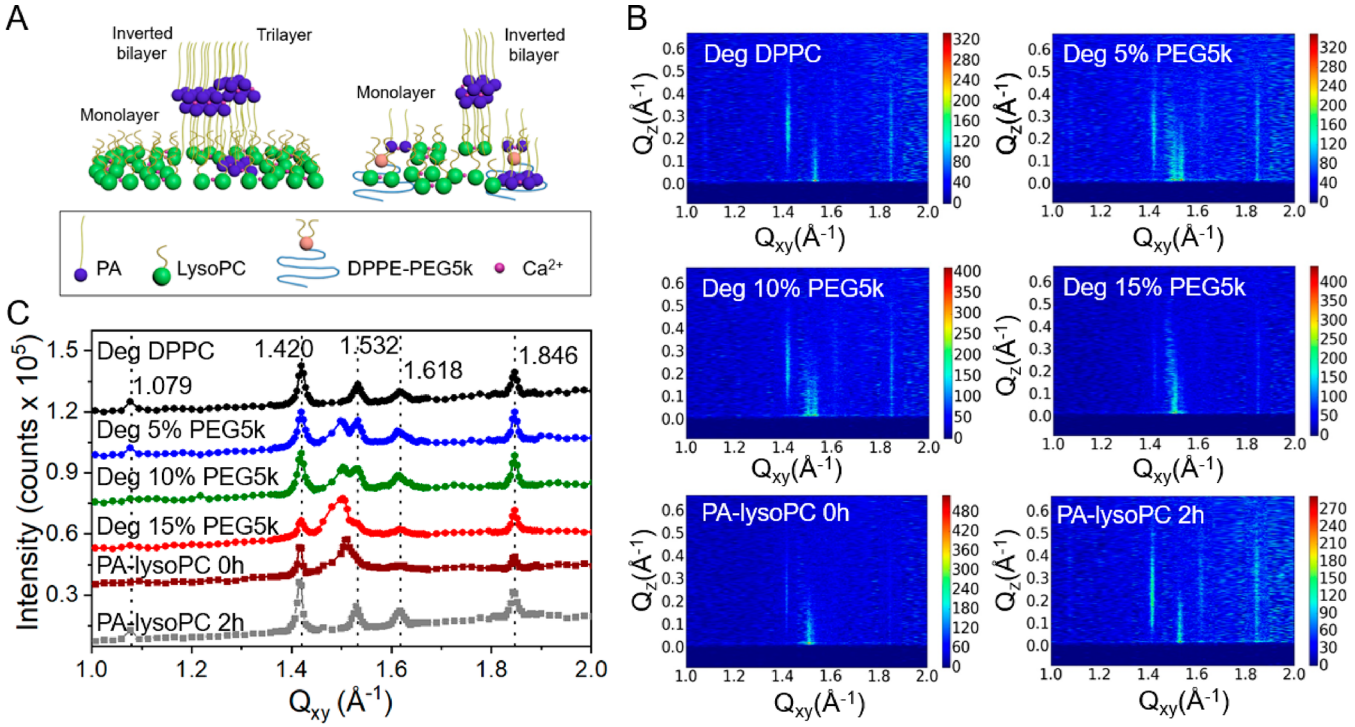

Figure 4. Molecular organization parallel to gas−liquid interface after film degradation. (A) Schematics for degraded DPPC and degraded PEGylated DPPC films. (B) Two-dimensional GIXD results and (C) Bragg peaks of films consisting of DPPC and DPPC with 5%, 10%, and 15% PEG5K after lipid degradation. The Bragg peaks of the PA-lysoPC mixture on the Ca buffer immediately after surface pressure reached 10 mN/m and after being maintained at 10 mN/m for 2 h are also shown for comparison. The black dashed lines indicate the peak positions of the degraded DPPC film. Their values are specified with a unit of $Å^{-1}$. Data are offset for clarity.

lateral interfacial organization of DPPC monolayers in the C phase.

With the inclusion of DPPE-PEG5k in the monolayers, XR data displayed an additional peak at a low Q_z just beyond the critical angle, and the peak intensity increased with the increased ratio of DPPE-PEG5k in the monolayer (Figure 2C). The peaks at such a low Q_z represented the accumulated PEG moieties underneath the lipid headgroup regions. The long decays of the electron density profiles between the lipid headgroup and the subphase buffer indicate the brush configuration of PEG (Figure 2D and Table 1), which is consistent with the brief theoretical analysis. The Flory radius, R_F, for PEG (M_w 5k) in an aqueous solution is about 67 Å.[43,44] According to the scaling model proposed by De Gennes[45] for grafted polymers, when the distance between grafting sites, D, is smaller than $2R_F$, the brush regime applied. With 5%, 10%, and 15% of PEGylated lipids at the interface in the condensed phase, the average distance of the PEG sites is estimated to be about 30, 21, and 17 Å, respectively, as follows,

$$D \approx \sqrt{S/\phi}$$

where S is the average area per molecule (which is about 45 $Å^2$ at a surface pressure of 25 mN/m), and ϕ is the percentage of PEG. In these cases, D is much smaller than $2R_F$. The thickness of the PEG layer was calculated to be about 120 Å from fitting the experimental data, similar to the reported PEG brush length of 115 Å in a membrane of 1,2-distearoyl-*sn*-glycero-3-phosphocholine (DSPC) with 5% DSPE-PEG5k by Kenworthy.[46]

Except for the PEG-induced peaks at low Q_z, the reflectivity curves of DPPC with different molar fractions of DPPE-PEG5k were similar, as were the electron density profiles for the lipid tail and headgroup regions. This confirms that including DPPE-PEG5k up to 15% in the monolayer had minimal effect on DPPC packing in the C phase.

Isotherm, GIXD, and XR results consistently showed that the observed degree of PEGylation had limited effects on the interfacial organization of DPPC monolayers in the C phase, suggesting that the PEG moieties were mostly excluded from the phospholipid layers. However, in the studies by Majewski et al.[21,22] on the interfacial organization of DSPE monolayers at about 40 mN/m, addition of DSPE-PEG2k appeared to induce protrusion of the surrounding phospholipid molecules into the subphase. The different findings of these researchers may be attributed to the different head groups of the lipids used in their studies. Compared to PC with a neutral bulky headgroup and cylindrical shape, PE has a smaller negatively charged headgroup and a truncated conical shape. As a result, at a high surface pressure, PE molecules may have a stronger tendency than PC molecules to protrude from the planar monolayer. In our study of DPPC and DPPE-PEG5k monolayers, no such protrusion was observed, consistent with Stepniewski et al.'s simulation results for a binary mixture of DSPC and DSPE-PEG2k.[47]

Effects of PEGylation on $sPLA_2$ adsorption. After $sPLA_2$ was added to the subphase of the Ca-free buffer, the surface pressure of the monolayers dropped from 25 to about 16 mN/m and slowly reached quasi-equilibrium within two hours. This is due to film relaxation since the experimental conditions changed from a constant pressure to a constant area. XR results for DPPC and DPPC with 5%, 10%, and 15% DPPE-PEG5k monolayers after $sPLA_2$ adsorption are plotted in Figure 3A, which are compared with the XR curve for the DPPC monolayer before $sPLA_2$ adsorption on the Ca-free

https://dx.doi.org/10.1021/acs.langmuir.0c01202
Langmuir 2020, 36, 7573−7581

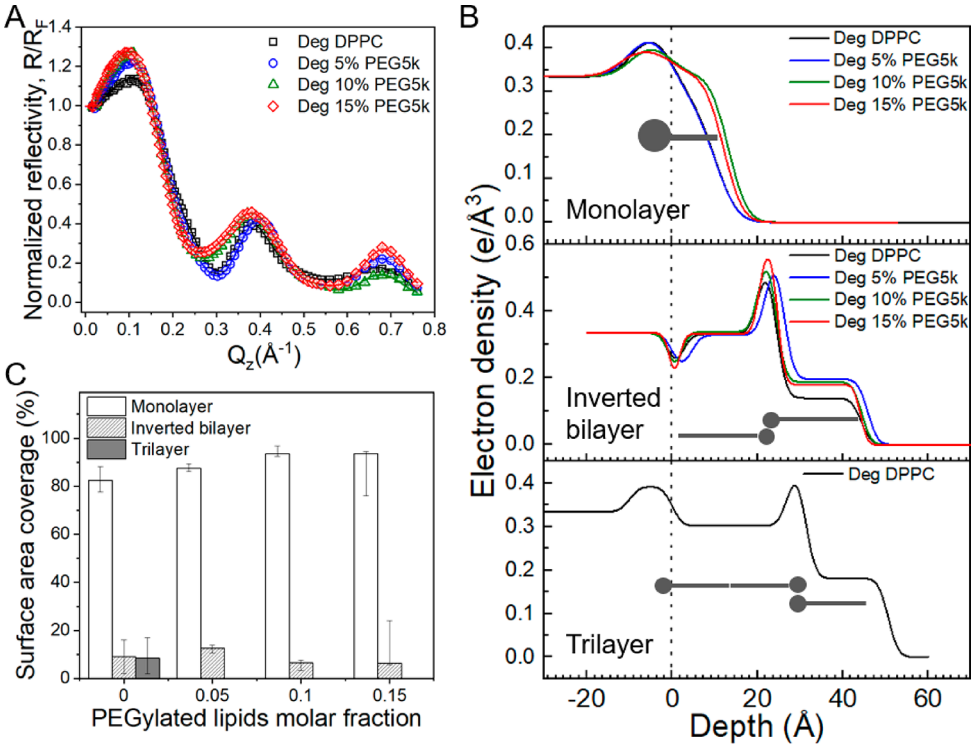

Figure 5. Organization of molecules normal to the gas−liquid interface after film degradation. (A) Normalized X-ray reflectivity for degraded DPPC and DPPC with 5%, 10%, and 15% DPPE-PEG5k films. (B) Electron density profiles of different domains calculated from the multiphase box model fitting. The electron density profiles aligned at the zero position of the gas−liquid interface (indicated by the vertical black dotted line). (C) Percentage of surface area coverage of the monolayer, inverted bilayer, and trilayer domains.

buffer. The electron density profiles corresponding to the best fits of the curves in Figure 3A (the solid lines) are plotted in Figure 3B, and the structural parameters are listed in Table S2. In comparison with the electron density of the pure DPPC monolayer, after $sPLA_2$ adsorption, the electron density in the DPPC tail region increased and an additional layer with an electron density of 0.34 e/Å^3 appeared under the headgroup region (the black solid line in Figure 3B), suggesting adsorption of $sPLA_2$ to the DPPC monolayer. When including PEGylated lipid into the monolayer films, the electron density profiles were very similar, indicating minimal effects of PEG on $sPLA_2$ adsorption.

After enzyme adsorption, the alkyl tails of lipids in all four monolayers maintained the NN packing structure, but the positions of the GIXD peaks shifted. In Figure 3C, the gray dashed lines indicate the peak positions of DPPC Bragg peaks before adsorption, and the black dotted lines indicated its peak positions after $sPLA_2$ adsorption. Bragg peaks shifted in the higher Q_{xy} direction and the out-plane Bragg rod shifted in the lower Q_z direction, indicating tighter and less tilted packing structures of lipid molecules induced by the adsorption of $sPLA_2$ to the monolayers. However, PEGylation had negligible effects on the decrease in the mean molecular area and the tilt angle induced by $sPLA_2$ adsorption (Figure 3D). The structural parameters obtained from GIXD are listed in Table S3.

Effects of PEGylation on Fatty Acid and lyso PC Reorganization after Lipid Degradation. After $sPLA_2$ was added to the subphase of the Ca buffer, it catalyzed the degradation of the lipids and caused a continuous drop in the surface pressure (Figure s1). All the films were exposed to $sPLA_2$ for 2 h before the XR and GIXD measurements on the degraded films. Our previous studies showed that after DPPC degradation, the interface was covered by monolayer liquid-phase domains of lysoPC accompanied by highly ordered inverted bilayer and trilayer domains of PA-Ca^{2+} complexes with oblique packing structures.[32−34] The degraded films of DPPC with different amounts of DPPE-PEG5k also contained monolayer domains mixed with inverted bilayer domains of PA-Ca^{2+} complexes; however, trilayer domains were not detectable, and a remarkable amount of PA molecules maintained hexagonal packing in the monolayer domains (Figure 4).

Specifically, after DPPC degradation, the two Bragg peaks representing the NN tilted lateral packing of the DPPC alkyl tails were replaced by five new and strong Bragg peaks (indicated by the dash vertical lines in Figure 4C). The corresponding peak positions are also listed in Table S4. The positions and intensity ratios of the five Bragg peaks obtained from the degraded DPPC film were similar to those of peaks obtained from a PA film on the same Ca buffer.[32,33] When including 5% or 10% DPPE-PEG5k in the films, an additional in-plane peak emerged at 1.5 Å^{-1} (Figure 4B and C). Further increasing the molar fraction of DPPE-PEG5k to 15% resulted in more pronounced intensity of this single in-plane peak (Figure 4B and C). This in-plane peak indicated a hexagonal packing structure of monolayer PA alkyl tails with a unit cell area of about 20.2 Å^2, which was similar to the hexagonal structure of a pure PA film detected on water at 30 mN/m.[48] At the same time, the intensity of all other peaks decreased. In particular, the peak at about 1.08 Å^{-1}, which was scattered from the organized Ca^{2+} packing structures, became too weak to discern.

https://dx.doi.org/10.1021/acs.langmuir.0c01202
Langmuir 2020, 36, 7573−7581

In order to further interpret the GIXD results for the film of degraded DPPC with 15% DPPE-PEG5k, a film of PA and lysoPC at a 1:1 molecular ratio was prepared on the Ca buffer. Immediately after the surface pressure reached 10 mN/m, GIXD measurements were conducted. The initial Bragg peak distribution was similar to that of the film of degraded DPPC with 15% DPPE-PEG5k (Figure 4B and C). After the film of PA and lysoPC was maintained at a constant pressure of 10 mN/m for two hours, the GIXD measurement was conducted again, and the Bragg peak distribution became similar to that of the degraded DPPC film. Therefore, the PA-lysoPC film was undergoing a kinetic process and the molecular packing of PA transited from hexagonal to oblique PA-Ca^{2+} complex structures. For the PEGylated films, over time, their GIXD Bragg peaks became similar to those of the degraded DPPC film, suggesting that PEGylation hindered molecule reorganization and delayed the formation of PA−Ca^{2+} complex structures at the interface.

The vertical structure of the films after lipid degradation was analyzed (Figure 5). The corresponding structural parameters are listed in Table s5. For the degraded films consisting of DPPE-PEG5k, a two-phase box model containing inverted bilayer and monolayer domains best fitted the XR data, suggesting that no substantial trilayer domains were present. Increasing the amount of DPPE-PEG5k in the film, the surface coverage of the monolayer domains increased, while the coverage of the inverted bilayer domains decreased (Figure 5C). In order to form the highly organized PA−Ca^{2+} bilayer domains, the PA molecules first needs to self-assemble. Therefore, PEG hindered the reorganization of PA molecules in the films and microphase separation and thus delayed the formation of the PA−Ca^{2+} multilayer structures.

In the monolayer domains, the electron density profiles of the degraded DPPC and DPPC with 5% DPPE-PEG5k are similar (top plot in Figure 5B). However, at higher molar fractions of PEG (10% or 15%), the electron density profiles of the degraded films are different, having longer tails with higher electron densities and similar headgroup thicknesses but lower electron densities. On the basis of the fact that PA has smaller head groups but more tightly packed tail groups compared to lysoPC, the observation of the electron density profiles of the monolayer domains indicated that with high PEGylation (above 10%), a remarkable amount of PA molecules remained in the monolayer domain together with lysoPC, while for degraded DPPC or DPPC with 5% DPPE-PEG, the monolayer domains mainly consisted of lysoPC. The electron densities of the inverted bilayer domains for all four degraded films are similar (the middle plot in Figure 5B), which indicates similar interfacial organization of PA−Ca^{2+} complexes. This result is also supported by the five similar GIXD peaks of the PA−Ca^{2+} complexes observed after the degradation of all four films.

Sustained release of encapsulated drugs from PEGylated lipid vesicles, compared to the vesicles without PEG conjugation, has been reported.[49,50] Enzyme-catalyzed degradation of the lipids results in the formation of the heterogeneous structures of loosely packed lysoPC and highly organized multilayer domains of PA−Ca^{2+} complexes, which induces the holes on the vesicles and thus causes leakage of the encapsulated drug.[32,33,51] The impeding effects of PEG conjugation on lysoPC and PA microphase separation and thus the formation of the heterogeneous structures provide a possible mechanistic explanation of the sustained drug release from PEGylated lipid vesicles.

CONCLUSIONS

The effects of PEGylation on phospholipid packing and degradation catalyzed by a phospholipase at the planar gas−liquid interface were directly quantified with molecular-level resolution. An extended layer of hydrophilic polymer brushes of PEG5k (at 5%, 10%, and 15%) exhibited limited effects on the molecular packing of DPPC monolayer in the C phase and negligible effects on $sPLA_2$ adsorption at the interface. However, conjugation of the polymer with the lipid hindered molecule reorganization, microphase separation of PA and lysoPC, and thus self-assembly of highly ordered PA−Ca^{2+} multilayer structures, which provides a possible explanation for the in vitro experimental observations that PEGylation sustained drug release from lipid vesicles. Information on the effects of PEGylation on molecular packing and interaction is essential for a mechanism-orientated design and optimization of polymer-grafted lipid vesicles.

ASSOCIATED CONTENT

Supporting Information

The Supporting Information is available free of charge at https://pubs.acs.org/doi/10.1021/acs.langmuir.0c01202.

Table of structural parameters obtained from GIXD measurements for monolayers; tables of structural parameters obtained from GIXD and XR measurements for monolayers with $sPLA_2$ adsorption, figure of surface pressure changes of lipid films during lipid degradation; and tables of structural parameters obtained from GIXD and XR measurements for the lipid films after $sPLA_2$-catalyzed degradation (PDF)

AUTHOR INFORMATION

Corresponding Author

Ying Liu − *Department of Chemical Engineering and Richard & Loan Hill Department of Bioengineering, University of Illinois at Chicago, Chicago, Illinois 60608, United States;* orcid.org/0000-0002-1207-8409; Email: liuying@uic.edu

Authors

Pin Zhang − *Department of Chemical Engineering, University of Illinois at Chicago, Chicago, Illinois 60608, United States;* orcid.org/0000-0003-0107-221X

Tiep Pham − *Department of Chemical Engineering, University of Illinois at Chicago, Chicago, Illinois 60608, United States*

Chang Liu − *Department of Chemical Engineering, University of Illinois at Chicago, Chicago, Illinois 60608, United States;* orcid.org/0000-0001-5271-9867

Paola Leon Plata − *Department of Chemical Engineering, University of Illinois at Chicago, Chicago, Illinois 60608, United States*

Joseph Kalkowski − *Department of Chemical Engineering, University of Illinois at Chicago, Chicago, Illinois 60608, United States*

Gang Cheng − *Department of Chemical Engineering, University of Illinois at Chicago, Chicago, Illinois 60608, United States;* orcid.org/0000-0002-7170-8968

Wei Bu − *NSF's ChemMatCARS, University of Chicago, Chicago, Illinois 60637, United States*

Binhua Lin − *NSF's ChemMatCARS, University of Chicago, Chicago, Illinois 60637, United States;* orcid.org/0000-0001-5932-4905

Complete contact information is available at:

https://dx.doi.org/10.1021/acs.langmuir.0c01202
Langmuir 2020, 36, 7573−7581

https://pubs.acs.org/10.1021/acs.langmuir.0c01202

Notes

The authors declare no competing financial interest.

■ ACKNOWLEDGMENTS

The study is supported by the NSF Nanomanufacturing Program (NSF CAREER #1350731). ChemMatCARS Sector 15 is principally supported by the Divisions of Chemistry (CHE) and Materials Research (DMR), National Science Foundation, under grant number NSF/CHE-1834750. Use of the Advanced Photon Source, an Office of Science User Facility operated for the U.S. Department of Energy (DOE) Office of Science by Argonne National Laboratory, was supported by the U.S. DOE under Contract No. DE-AC02-06CH11357. The authors thank Professor Mark L. Schlossman for many helpful discussions. The authors are grateful to Professor Ursula Perez-Salas for access to the Langmuir trough in her laboratory.

■ REFERENCES

(1) Webster, R.; Didier, E.; Harris, P.; Siegel, N.; Stadler, J.; Tilbury, L.; Smith, D. PEGylated Proteins: Evaluation of Their Safety in the Absence of Definitive Metabolism Studies. *Drug Metab. Dispos.* **2007**, *35* (1), 9−16.

(2) Lin, C.-C.; Anseth, K. S. PEG Hydrogels for the Controlled Release of Biomolecules in Regenerative Medicine. *Pharm. Res.* **2009**, *26* (3), 631−643.

(3) Carpenter, C. P.; Woodside, M. D.; Kinkead, E. R.; King, J. M.; Sullivan, L. J. Response of dogs to repeated intravenous injection of polyethylene glycol 4000 with notes on excretion and sensitization. *Toxicol. Appl. Pharmacol.* **1971**, *18* (1), 35−40.

(4) Drummond, D. C.; Meyer, O.; Hong, K.; Kirpotin, D. B.; Papahadjopoulos, D. Optimizing Liposomes for Delivery of Chemotherapeutic Agents to Solid Tumors. *Pharmacol. Rev.* **1999**, *51* (4), 691−744.

(5) Harris, J. M.; Chess, R. B. Effect of pegylation on pharmaceuticals. *Nat. Rev. Drug Discovery* **2003**, *2*, 214.

(6) Allen, C.; Dos Santos, N.; Gallagher, R.; Chiu, G.; Shu, Y.; Li, W.; Johnstone, S. a.; Janoff, A.; Mayer, L.; Webb, M.; et al. , Controlling the physical behavior and biological performance of liposome formulations through use of surface grafted poly (ethylene glycol). *Biosci. Rep.* **2002**, *22* (2), 225−250.

(7) Malmsten, M.; Emoto, K.; Van Alstine, J. M. Effect of Chain Density on Inhibition of Protein Adsorption by Poly(ethylene glycol) Based Coatings. *J. Colloid Interface Sci.* **1998**, *202* (2), 507−517.

(8) Suk, J. S.; Xu, Q.; Kim, N.; Hanes, J.; Ensign, L. M. PEGylation as a strategy for improving nanoparticle-based drug and gene delivery. *Adv. Drug Delivery Rev.* **2016**, *99*, 28−51.

(9) Blume, G.; Cevc, G. Molecular mechanism of the lipid vesicle longevity in vivo. *Biochim. Biophys. Acta, Biomembr.* **1993**, *1146* (2), 157−168.

(10) Lee, H.; Larson, R. G. Adsorption of Plasma Proteins onto PEGylated Lipid Bilayers: The Effect of PEG Size and Grafting Density. *Biomacromolecules* **2016**, *17* (5), 1757−1765.

(11) Du, H.; Chandaroy, P.; Hui, S. W. Grafted poly-(ethylene glycol) on lipid surfaces inhibits protein adsorption and cell adhesion. *Biochim. Biophys. Acta, Biomembr.* **1997**, *1326* (2), 236−248.

(12) Needham, D.; McIntosh, T. J.; Lasic, D. D. Repulsive interactions and mechanical stability of polymer-grafted lipid membranes. *Biochim. Biophys. Acta, Biomembr.* **1992**, *1108* (1), 40−48.

(13) Dos Santos, N.; Allen, C.; Doppen, A.-M.; Anantha, M.; Cox, K. A. K.; Gallagher, R. C.; Karlsson, G.; Edwards, K.; Kenner, G.; Samuels, L.; Webb, M. S.; Bally, M. B. Influence of poly(ethylene glycol) grafting density and polymer length on liposomes: Relating plasma circulation lifetimes to protein binding. *Biochim. Biophys. Acta, Biomembr.* **2007**, *1768* (6), 1367−1377.

(14) Ahl, P. L.; Bhatia, S. K.; Meers, P.; Roberts, P.; Stevens, R.; Dause, R.; Perkins, W. R.; Janoff, A. S. Enhancement of the in vivo circulation lifetime of l-α-distearoylphosphatidylcholine liposomes: importance of liposomal aggregation versus complement opsonization. *Biochim. Biophys. Acta, Biomembr.* **1997**, *1329* (2), 370−382.

(15) Vert, M.; Domurado, D. Poly (ethylene glycol): Protein-repulsive or albumin-compatible? *J. Biomater. Sci., Polym. Ed.* **2000**, *11* (12), 1307−1317.

(16) Schöttler, S.; Becker, G.; Winzen, S.; Steinbach, T.; Mohr, K.; Landfester, K.; Mailänder, V.; Wurm, F. R. Protein adsorption is required for stealth effect of poly(ethylene glycol)- and poly-(phosphoester)-coated nanocarriers. *Nat. Nanotechnol.* **2016**, *11*, 372.

(17) Jørgensen, K.; Vermehren, C.; Mouritsen, O. G. Enhancement of phospholipase A2 catalyzed degradation of polymer grafted PEG-liposomes: effects of lipopolymer-concentration and chain-length. *Pharm. Res.* **1999**, *16* (9), 1491−1493.

(18) Vermehren, C.; Kiebler, T.; Hylander, I.; Callisen, T. H.; Jørgensen, K. Increase in phospholipase A2 activity towards lipopolymer-containing liposomes. *Biochim. Biophys. Acta, Biomembr.* **1998**, *1373* (1), 27−36.

(19) Davidsen, J.; Vermehren, C.; Frøkjær, S.; Mouritsen, O. G.; Jørgensen, K. Enzymatic degradation of polymer covered SOPC-liposomes in relation to drug delivery. *Adv. Colloid Interface Sci.* **2001**, *89−90*, 303−311.

(20) Zhu, G.; Mock, J. N.; Aljuffali, I.; Cummings, B. S.; Arnold, R. D. Secretory phospholipase A2 responsive liposomes. *J. Pharm. Sci.* **2011**, *100* (8), 3146−3159.

(21) Majewski, J.; Kuhl, T.; Kjaer, K.; Gerstenberg, M.; Als-Nielsen, J.; Israelachvili, J.; Smith, G. X-ray synchrotron study of packing and protrusions of polymer-lipid monolayers at the air-water interface. *J. Am. Chem. Soc.* **1998**, *120* (7), 1469−1473.

(22) Majewski, J.; Kuhl, T. L.; Gerstenberg, M. C.; Israelachvili, J. N.; Smith, G. S. Structure of Phospholipid Monolayers Containing Poly(ethylene glycol) Lipids at the Air−Water Interface. *J. Phys. Chem. B* **1997**, *101* (16), 3122−3129.

(23) Halperin, A.; Mouritsen, O. G. Role of lipid protrusions in the function of interfacial enzymes. *Eur. Biophys. J.* **2005**, *34* (7), 967−971.

(24) Malinin, V. S.; Frederik, P.; Lentz, B. R. Osmotic and curvature stress affect PEG-induced fusion of lipid vesicles but not mixing of their lipids. *Biophys. J.* **2002**, *82* (4), 2090−2100.

(25) Lee, H.; Pastor, R. W. Coarse-Grained Model for PEGylated Lipids: Effect of PEGylation on the Size and Shape of Self-Assembled Structures. *J. Phys. Chem. B* **2011**, *115* (24), 7830−7837.

(26) Garbuzenko, O.; Barenholz, Y.; Priev, A. Effect of grafted PEG on liposome size and on compressibility and packing of lipid bilayer. *Chem. Phys. Lipids* **2005**, *135* (2), 117−129.

(27) Johnsson, M.; Edwards, K. Liposomes, disks, and spherical micelles: aggregate structure in mixtures of gel phase phosphatidylcholines and poly (ethylene glycol)-phospholipids. *Biophys. J.* **2003**, *85* (6), 3839−3847.

(28) Lichtenberg, D.; Romero, G.; Menashe, M.; Biltonen, R. L. Hydrolysis of dipalmitoylphosphatidylcholine large unilamellar vesicles by porcine pancreatic phospholipase A2. *J. Biol. Chem.* **1986**, *261* (12), 5334−5340.

(29) Davidsen, J.; Jørgensen, K.; Andresen, T. L.; Mouritsen, O. G. Secreted phospholipase A2 as a new enzymatic trigger mechanism for localised liposomal drug release and absorption in diseased tissue. *Biochim. Biophys. Acta, Biomembr.* **2003**, *1609* (1), 95−101.

(30) Donovan, A. J.; Kalkowski, J.; Szymusiak, M.; Wang, C.; Smith, S. A.; Klie, R. F.; Morrissey, J. H.; Liu, Y. Artificial dense granules: a procoagulant liposomal formulation modeled after platelet polyphosphate storage pools. *Biomacromolecules* **2016**, *17* (8), 2572−2581.

(31) Donovan, A. J.; Kalkowski, J.; Smith, S. A.; Morrissey, J. H.; Liu, Y. Size-controlled synthesis of granular polyphosphate nano-

particles at physiologic salt concentrations for blood clotting. *Biomacromolecules* **2014**, *15* (11), 3976−3984.
(32) Zhang, P.; Villanueva, V.; Kalkowski, J.; Liu, C.; Donovan, A. J.; Bu, W.; Schlossman, M. L.; Lin, B.; Liu, Y. Molecular interactions of phospholipid monolayers with a model phospholipase. *Soft Matter* **2019**, *15* (20), 4068−4077.
(33) Zhang, P.; Villanueva, V.; Kalkowski, J.; Liu, C.; Pham, T.; Perez-Salas, U.; Bu, W.; Lin, B.; Liu, Y. Polyunsaturated Phospholipid Modified Membrane Degradation Catalyzed by a Secreted Phospholipase A2. *Langmuir* **2019**, *35* (36), 11643−11650.
(34) Zhang, P.; Pham, T.; Zheng, X.; Liu, C.; Plata, P. L.; Král, P.; Bu, W.; Lin, B.; Liu, Y. Spontaneous collapse of palmitic acid films on an alkaline buffer containing calcium ions. *Colloids Surf., B* **2020**, *193*, 111100.
(35) Málková, Š.; Long, F.; Stahelin, R. V.; Pingali, S. V.; Murray, D.; Cho, W.; Schlossman, M. L. X-Ray Reflectivity Studies of cPLA 2 α-C2 Domains Adsorbed onto Langmuir Monolayers of SOPC. *Biophys. J.* **2005**, *89* (3), 1861−1873.
(36) Parratt, L. G. Surface studies of solids by total reflection of X-rays. *Phys. Rev.* **1954**, *95* (2), 359−369.
(37) Tikhonov, A. M.; Pingali, S. V.; Schlossman, M. L. Molecular ordering and phase transitions in alkanol monolayers at the water−hexane interface. *J. Chem. Phys.* **2004**, *120* (24), 11822−11838.
(38) Kjaer, K.; Als-Nielsen, J.; Helm, C. A.; Laxhuber, L. A.; Möhwald, H. Ordering in Lipid Monolayers Studied by Synchrotron X-Ray Diffraction and Fluorescence Microscopy. *Phys. Rev. Lett.* **1987**, *58* (21), 2224−2227.
(39) Dutta, P.; Peng, J. B.; Lin, B.; Ketterson, J. B.; Prakash, M.; Georgopoulos, P.; Ehrlich, S. X-Ray Diffraction Studies of Organic Monolayers on the Surface of Water. *Phys. Rev. Lett.* **1987**, *58* (21), 2228−2231.
(40) Bu, W.; Vaknin, D. Bilayer and Trilayer Crystalline Formation by Collapsing Behenic Acid Monolayers at Gas/Aqueous Interfaces. *Langmuir* **2008**, *24* (2), 441−447.
(41) Kaganer, V. M.; Möhwald, H.; Dutta, P. Structure and phase transitions in Langmuir monolayers. *Rev. Mod. Phys.* **1999**, *71* (3), 779−819.
(42) Tanwir, K.; Shahid, M. N.; Thomas, A.; Tsoukanova, V. Coexisting Phases in PEGylated Phosphocholine Membranes: A Model Study. *Langmuir* **2012**, *28* (39), 14000−14009.
(43) Marsh, D.; Bartucci, R.; Sportelli, L. Lipid membranes with grafted polymers: physicochemical aspects. *Biochim. Biophys. Acta, Biomembr.* **2003**, *1615* (1), 33−59.
(44) Flory, P. J. *Principles of Polymer Chemistry*; Cornell University Press: 1953.
(45) de Gennes, P. G. Conformations of Polymers Attached to an Interface. *Macromolecules* **1980**, *13* (5), 1069−1075.
(46) Kenworthy, A. K.; Hristova, K.; Needham, D.; McIntosh, T. J. Range and magnitude of the steric pressure between bilayers containing phospholipids with covalently attached poly(ethylene glycol). *Biophys. J.* **1995**, *68* (5), 1921−1936.
(47) Stepniewski, M.; Pasenkiewicz-Gierula, M.; Róg, T.; Danne, R.; Orlowski, A.; Karttunen, M.; Urtti, A.; Yliperttula, M.; Vuorimaa, E.; Bunker, A. Study of PEGylated lipid layers as a model for PEGylated liposome surfaces: molecular dynamics simulation and Langmuir monolayer studies. *Langmuir* **2011**, *27* (12), 7788−7798.
(48) Lee, K. Y. C.; Gopal, A.; von Nahmen, A.; Zasadzinski, J. A.; Majewski, J.; Smith, G. S.; Howes, P. B.; Kjaer, K. Influence of palmitic acid and hexadecanol on the phase transition temperature and molecular packing of dipalmitoylphosphatidyl-choline monolayers at the air−water interface. *J. Chem. Phys.* **2002**, *116* (2), 774−783.
(49) Blume, G.; Cevc, G. Liposomes for the sustained drug release in vivo. *Biochim. Biophys. Acta, Biomembr.* **1990**, *1029* (1), 91−97.
(50) Kim, J.-Y.; Kim, J.-K.; Park, J.-S.; Byun, Y.; Kim, C.-K. The use of PEGylated liposomes to prolong circulation lifetimes of tissue plasminogen activator. *Biomaterials* **2009**, *30* (29), 5751−5756.
(51) Agafonov, A.; Gritsenko, E.; Belosludtsev, K.; Kovalev, A.; Gateau-Roesch, O.; Saris, N.-E. L.; Mironova, G. D. A permeability transition in liposomes induced by the formation of Ca2+/palmitic acid complexes. *Biochim. Biophys. Acta, Biomembr.* **2003**, *1609* (2), 153−160.

https://dx.doi.org/10.1021/acs.langmuir.0c01202
Langmuir 2020, 36, 7573−7581